Photoionization of the Be isoelectronic sequence from the ground and the ^1S bound excited states

T. N. Chang and Lizhi Zhu
Department of Physics and Astronomy, University of Southern California, Los Angeles, California 90089-0484
(Received 28 February 1994)

Theoretical photoionization spectra below the $2p$ threshold of the Be isoelectronic sequence from the ground and a few selected ^1S bound excited states are calculated using a B-spline-based configuration-interaction approach. The resonant structures of the doubly excited autoionization series following photoionization from different initial states are analyzed in detail in terms of various initial- and final-state multielectron interactions. In addition, our calculation has shown that the resonant widths vary smoothly as functions of the effective principal quantum number ν along the autoionization series and approach approximately an expected ν^{-3} dependence as ν increases.

PACS number(s): 32.80.Fb, 32.80.Dz, 31.20.Tz, 32.70.Jz

I. INTRODUCTION

Recent development of ion sources, using sophisticated ion trap techniques [1] and accelerator-based technology such as the electron-beam ion source [2] and electron-beam ion trap [3], have opened up the possibility for a detailed study of atomic transitions of atomic ions under a more controlled environment. A more advanced application of the synchrotron radiation using insertion devices has further extended the continuum light source into a shorter wavelength region for a more elaborate experimental study of atomic ions [4]. On the application side, detailed studies of atomic processes in plasmas have shown that many atomic transitions are strongly affected by the multistep processes involving resonances dominated by multiple excitations. For instance, in high-temperature low-density plasmas, the electron-ion recombination is dominated by the radiative electron capture represented by

$$e^- + A^{+(\rho+1)}(\alpha) \rightarrow A^{+\rho}(\mu,\nu)^{**} \rightarrow A^{+\rho}(\alpha,\beta)^* + \hbar\omega \ , \tag{1}$$

where an incoming electron is captured by an atomic ion of a net effective nuclear charge $Z_{\text{eff}}=\rho+1$, with its outer electron represented by an electronic configuration α. A photon of energy $\hbar\omega$ is emitted from a doubly excited intermediate state dominated by an electronic configuration (μ,ν) of an ion with $Z_{\text{eff}}=\rho$, leaving the final ion of same charge $Z_{\text{eff}}=\rho$ in an excited state represented by an electronic configuration (α,β). Theoretically, the inverse of this process represents the photoionization from a bound excited state to a spectral region dominated by doubly excited autoionization states embedded in the continuum, such as the strongly energy-dependent resonant structures of a divalent atom (e.g., an alkaline-earth atom with two interacting valence electrons outside a closed-shell ^1S core) above its first ionization threshold.

For a light alkaline-earth atom, nearly all of the doubly excited states are located near or above the first ionization threshold and embedded in the one-electron ionization channel. For heavier alkaline-earth atoms, the mutual screening between the two simultaneously excited electrons of a doubly excited state becomes less complete than the screening experienced by the outer electron due to a radially separated inner electron of a singly bound excited state. Consequently, some of the doubly excited resonant states move below the ionization threshold and mix substantially with the singly excited states. The close proximity in energy between the singly and doubly excited bound states often alter the characteristics of the singly excited bound state through configuration mixing, leading to a significant energy shift and a noticeable redistribution of oscillator strengths (or radiative lifetime) involving the singly excited bound state [5]. Similar to the heavier alkaline-earth atoms, doubly excited states are also found to locate below the ionization threshold along the isoelectronic sequence of lighter alkaline-earth atoms, as the effective nuclear charge ρ increases even when ρ is considerably smaller than the one for a heavier alkaline-earth atom. As a result, the isoelectronic sequence of a light alkaline-earth atom represents an alternative but less complex system for a detailed study of multielectron interactions in photoionization from correlated bound excited states.

Physically, the interaction strength between the bound and continuum components of the state wave function of a doubly excited state is measured by the resonant width Γ, which also determines the nonradiative decay rate of an autoionization state. For an autoionization state of a divalent atom, representing a doubly excited $(n_i l_i \nu l_o)$ $^{2S+1}L_J$ bound component embedded in a singly ionized $(ns\epsilon l)$ $^{2S+1}L_J$ continuum background corresponding to an ionized l electron of energy ϵ, the resonant width Γ can be estimated approximately in terms of the Coulomb interaction between the bound and continuum components, i.e.,

$$\left| \langle (n_i l_i \nu l_0)^{2S+1}L_J | \frac{1}{r_{12}} | (ns\epsilon l)^{2S+1}L_J \rangle \right|^2 . \tag{2}$$

Following the standard quantum defect theory,[6,7] the ν dependence of the resonant widths Γ of a $(n_i l_i \nu l_o)$ $^{2S+1}L_J$ doubly excited autoionization series is approxi-

mately given by the ν dependence of the one-electron radial function of the νl_o orbit, if the range of the effective interaction r_0 is small. As a result, Γ approaches a ν^{-3} dependence as ν increases along the autoionization series [8].

On the other hand, the resonant profile, which is often expressed qualitatively by the Fano formula [6] in terms of an asymmetry parameter q, measures the interference between transitions from an initial state to the bound and continuum components of the final-state wave function. Unlike the resonant width Γ, which is independent of the initial state of a transition, the q parameter may, and often does, vary significantly for transitions starting from different initial states. In general, the q value is large and the resonant structure is approximately symmetric if the spectrum is dominated by the contribution from the transition to the bound component of the final-state wave function. If the contribution from transitions to both bound and continuum components of the final-state wave function is comparable, the resonant profile is asymmetric with an intermediate q value. If the spectrum is completely dominated by the transition to the continuum component of the final-state wave function, a near-zero cross section, or a window resonance, is expected either near or at the resonant energy E_r with $q \sim 0$.

One of the main purposes of this paper is to study in detail the variation of the resonant structure of individual doubly excited autoionization states resulting from photoionization originated from different initial states along the Be isoelectronic sequence. We are able to link the structure profile to the configuration mixing in the initial and final states of the photoionization by identifying the dominating transition of individual electron. In addition, we will verify the ν^{-3} dependence of the resonant widths Γ along the autoionization series as ν increases for the Be isoelectronic sequence.

II. THEORETICAL PROCEDURE

Our calculation employs a B-spline-based configuration-interaction method for the continuum (CIC) [9,10]. Briefly, all state wave functions, which represent both bound and continuum states, are expressed in terms of a finite L^2 basis set constructed from B-spline-based frozen-core Hartree-Fock (FCHF) one-particle orbital functions χ [11,12]. The FCHF orbital functions χ are confined in a sphere of radius R and subject to a Coulomb potential corresponding to a positive charge of $Z-2$ asymptotically for a Be-like ion of nuclear charge Z. Following the usual convention, all one-particle orbital functions χ start with positive values at $r=0$ in the present calculation. A parametrized long-range dipole core-polarization potential is also included to account for the intrashell core excitation and the intershell core-valence interaction [10,13]. Following the CIC procedure detailed elsewhere [9,10], an outgoing l electron with momentum k is represented by an oscillating numerical function $\xi_{\epsilon l}(r)$, which is matched at a finite but large r against an asymptotic expression [14]

$$\xi_{\epsilon l}(r) \rightarrow A \left[\frac{k}{\zeta(r)} \right]^{1/2} \sin[\phi(r)+\delta_l] , \tag{3}$$

where δ_l is the scattering phase shift due to the short-range interaction, $\epsilon=\frac{1}{2}k^2$, and ζ and ϕ are functions of r. As $r \rightarrow R$, $\zeta \rightarrow k$, and

$$\phi \rightarrow \left[kr + \frac{Z_{\text{eff}}}{k} \ln(2kr) - \frac{l\pi}{2} + \delta_C \right] , \tag{4}$$

where $Z_{\text{eff}}=Z-3$ is the effective nuclear charge experienced by the ionized electron, and δ_C is the Coulomb phase shift [9,10]. An accurate representation of the continuum component of the state wave function by a discretized basis set depends critically on the matching between the calculated radial function $\xi_{\epsilon l}(r)$ and the asymptotic expression given by Eq. (3) over an extended r with a constant amplitude A.

At energy close to the doubly excited autoionization state, the scattering phase shift δ_l increases rapidly by a total of π. The phase shifts at a set of closely populated energy eigenvalues E across the resonance are obtained by repeating our calculation at slightly varied values of R. The energy E_r and the width Γ of the resonance are determined by a least-square fit of the phase shifts to the usual expression [15,16]

$$\delta_l(E) = \sum_{i=0}^{2} a_i E^i + \tan^{-1} \frac{\Gamma/2}{E_r - E} . \tag{5}$$

Finally, the photoionization cross section (in unit of a_0^2) can be expressed in terms of the oscillator strength f_{EI} for absorption by the simple relation

$$\sigma = \frac{4\pi\alpha}{kA^2} f_{EI} , \tag{6}$$

where α is the fine structure constant and f_{EI} is calculated numerically following the same procedure for the bound-bound transitions given elsewhere [9,10,17].

Approximately 15 configuration series (a total of over 1300 configurations) are included in the initial- and final-state wave functions in the present B-spline-based CIC calculation. For the ^1S initial state, it is equivalent to a 15-state close-coupling calculation. For the ^1P final state, the present calculation approximates a ten-state close-coupling calculation.

III. RESULTS AND DISCUSSIONS

A. Photoionization spectra

Figure 1 represents the photoionization spectra from the ground state of Be-like B II, C III, N IV, O V, and F VI (i.e., $Z_{\text{eff}}=2-6$). Similar to the Be I and C III spectra reported recently [18], the ground-state photoionization is dominated by the narrow $2pnd\ ^1P$ and the $q \sim 0$ type $2pns\ ^1P$ resonances. The $2s\ ^2S$ threshold (i.e., the first ionization threshold) of N IV, O V, and F VI ions are indicated by the solid square in Fig. 1. Both $2s\ ^2S$ and $2p\ ^2P$ thresholds, listed together with the $2s^2\ ^1S$ ground state in

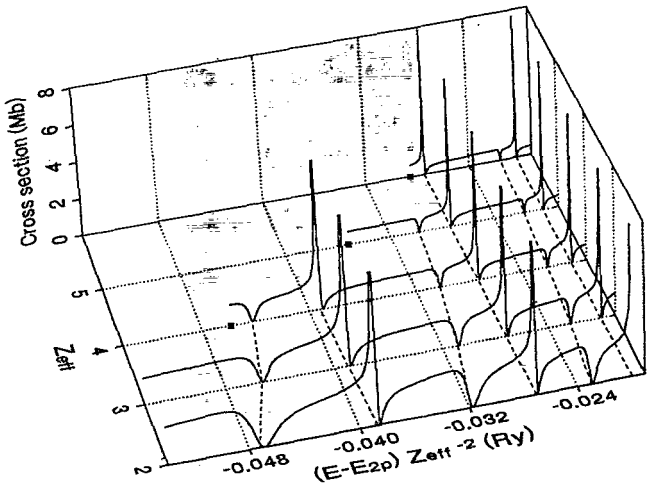

FIG. 1. Photoionization spectra from the $2s^2\,{}^1S$ ground state of Be-like B II, C III, N IV, O V, and F VI (i.e., $Z_{\rm eff}=2$–6). the $2s\,{}^2S$ ionization thresholds of N IV, O V, and F VI ions are indicated by the solid square. The $2s\,{}^2S$ ionization thresholds of B II and C III are below the energy scale shown. The energies of the $2pn(\geq 5)l\,{}^1P$ resonances are indicated by the dashed lines.

Table I, are measured against the double ionization threshold. Our calculation has shown that the energy separations between the $2p\,{}^2P$ threshold E_{2p} and the $2pn(\geq 5)l\,{}^1P$ resonances (indicated by the dashed lines in Fig. 1) scale approximately as $Z_{\rm eff}^2$.

The resonant profile of the $q\sim 0$-type $2pns\,{}^1P$ structures can be attributed directly to the near-zero bound-bound contribution to the oscillator strength from a mixture of $2s^2$ and $2p^2$ initial configurations to the $2pns$ final configuration. (For B II, the ground state is approximately a 92% and 8% mixture of $2s^2$ and $2p^2$ configurations.) The transition amplitude from the dominating $2s^2$ configuration to $2pn(\geq 3)l$ is very small due to the simultaneous change of electronic orbitals of both electrons. The transition from the small $2p^2$ mixture to $2pn(\geq 3)s$ corresponds essentially to a $2p\rightarrow ns$ one-electron process. Its near-zero transition amplitude is expected from the small oscillator strength known for the $2s2p\,{}^1P$ to $2sn(\geq 3)s\,{}^1S$ transition for Be and Be-like ions [12,20], which also corresponds to a $2p\rightarrow ns$ one-electron process.

TABLE I. Energy values (in Ry) for the $2s^2\,{}^1S$ ground state and the $2s\,{}^2S$ and $2p\,{}^2P$ thresholds measured against the double ionization threshold for the Be isoelectronic sequence. Data are taken from Ref. [19].

	$2s^2\,{}^1S$	$2s\,{}^2S$	$2p\,{}^2P$
Be	−2.023 82	−1.338 58	−1.047 56
B^+	−4.637 00	−2.787 99	−2.347 09
C^{2+}	−8.260 28	−4.740 43	−4.152 13
N^{3+}	−12.889 32	−7.195 04	−6.459 99
O^{4+}	−18.523 98	−10.151 86	−9.270 36
F^{5+}	−25.162 97	−13.611 59	−12.586 56
Ne^{6+}	−32.807 80	−17.572 90	−16.407 60
Na^{7+}	−41.460 54	−22.039 05	−20.711 00
Mg^{8+}	−51.111 12	−27.010 30	−25.527 95

With the bound-bound transition contributing substantially less than the $2s^2\rightarrow 2s\epsilon p$ bound-continuum transition, the zero cross section near E_r results directly from the sign change of the $2s\rightarrow\epsilon p$ one-electron bound-continuum dipole matrices $d_{sp}=\langle\xi_{\epsilon p}|r|\xi_{2s}\rangle$ due to the sign change of the one-electron oscillating function $\xi_{\epsilon p}$ at small r, shown in Fig. 2, as the scattering phase shift δ_p increases rapidly by a total of π across the resonance. The near-constant photoionization cross section on both side of the resonance can be attributed to the near-constant amplitude A of the one-electron oscillating function $\xi_{\epsilon p}$. In contrast, the bound-bound transition amplitude from the ground state to the $2pnd\,{}^1P$ resonance, primarily due to the $2p^2\rightarrow 2pnd$ excitation, is significantly greater than the amplitude of the $2p^2\rightarrow 2pns$ excitation in the ground state to $2pns\,{}^1P$ photoionization. This is also expected from the significantly larger oscillator strengths in the $2s2p\,{}^1P\rightarrow 2sn(\geq 3)d\,{}^1D$ excitation than in the $2s2p\,{}^1P\rightarrow 2sn(\geq 3)s\,{}^1S$ excitation for Be and Be-like ions [12,20]. Also, the asymmetric profile for the $2pnd\,{}^1P$ resonances shown in Fig. 1 indicates that contributions from the bound-bound $2p\rightarrow nd$ excitation and the bound-continuum $2s\rightarrow\epsilon p$ transition are comparable in magnitude.

Figure 3 represents the photoionization spectra from the $2p^2\,{}^1S$ bound excited state of Be-like B II, C III, N IV, O V, and F VI (i.e., $Z_{\rm eff}=2$–6). Although the final states are identical to those included in Fig. 1, the $q\sim 0$ type $2pns\,{}^1P$ resonances and the asymmetric $2pnd\,{}^1P$ resonances are both replaced by a fairly symmetric autoioni-

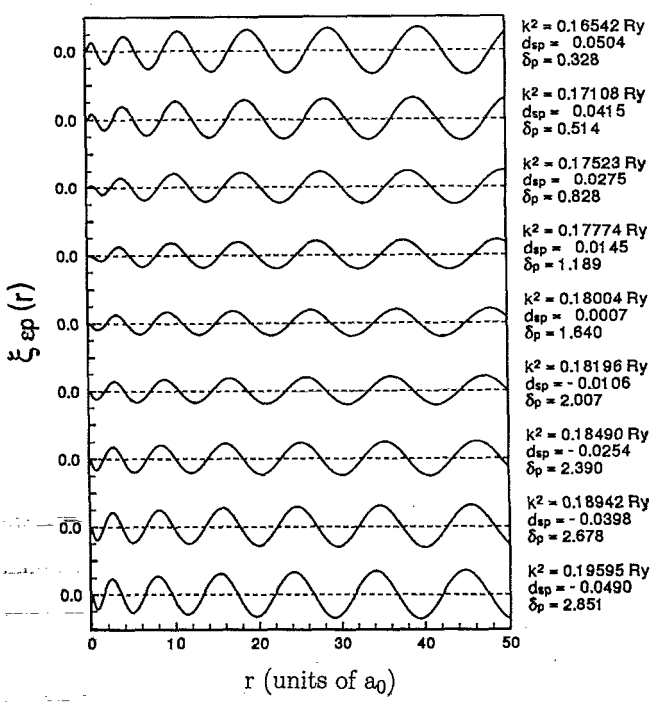

FIG. 2. The energy variation of the oscillating function $\xi_{\epsilon p}(r)$ [defined by Eq. (50) of Ref. [10]] across the $2p5s\,{}^1P$ resonance of Be-like C III at $\epsilon=k^2=0.179\,89$ Ry. The one-electron dipole matrix element $d_{\rm sp}=\langle\xi_{\epsilon p}|r|\xi_{2s}\rangle$ and the scattering phase shift δ_p are also given.

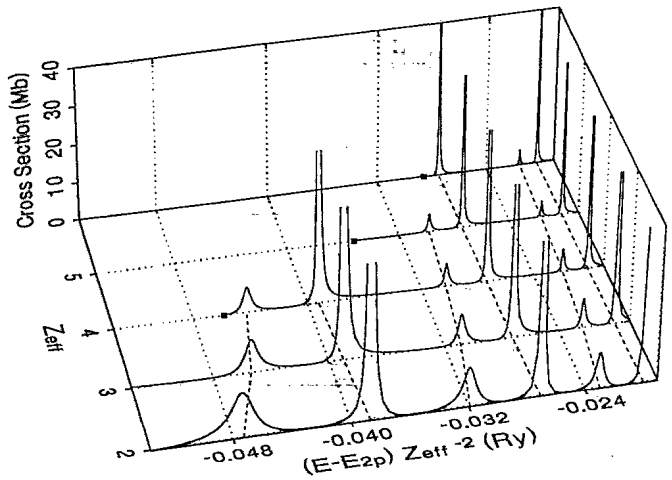

FIG. 3. Photoionization spectra from the $2p^2\,{}^1S$ state of Be-like B II, C III, N IV, O V, and F VI (i.e., $Z_{\text{eff}}=2$–6). The $2s\,{}^2S$ ionization thresholds of N IV, O V, and F VI ions are indicated by the solid square. The $2s\,{}^2S$ ionization thresholds of B II and C III are below the energy scale shown. The energies of the $2pn\,(\geq 5)l\,{}^1P$ resonances are indicated by the dashed lines.

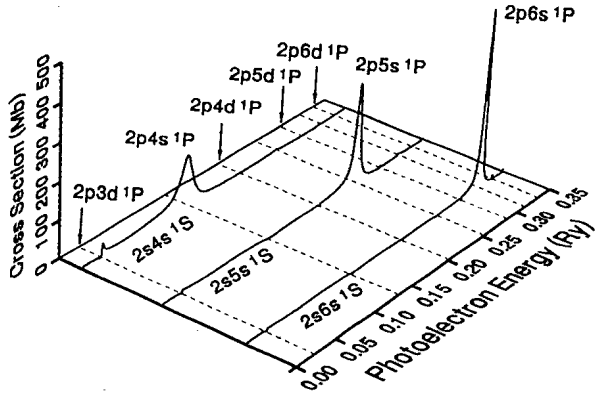

FIG. 5. Photoionization spectra from $2sn\,(4$–$6)s\,{}^1S$ excited states of Be-like B II.

zation structure. The main difference between the $2p^2\,{}^1S$ to $2pnl\,{}^1P$ and $2s^2\,{}^1S$ to $2pnl\,{}^1P$ transitions is the difference in their initial-state configuration mixing. Unlike the $2s^2\,{}^1S$ state, which is strongly dominated by the $2s^2$ configuration with a small $2p^2$ mixing, the $2p^2\,{}^1S$ state is only slightly dominated by the $2p^2$ configuration with a substantial $2sns$ mixing. (For instance, our calculation shows that the $2p^2$ and $2s3s$ mixing in the $2p^2\,{}^1S$ state of B II is approximately 54% and 46%, respectively.) Comparing to the $2s^2\,{}^1S$ to $2pns\,{}^1P$ photoionization, the relative bound-bound contribution from the $2p^2\rightarrow 2pns$ (or $2p\rightarrow ns$) excitation in the $2p^2\,{}^1S$ to $2pns\,{}^1P$ photoionization is substantially enhanced, while the relative bound-continuum contribution from the $2s3s\rightarrow 2s\epsilon p$ (or $3s\rightarrow\epsilon p$) transition is reduced. As a result, the oscillator strength is dominated by the $2p\rightarrow ns$ bound-bound excitation, leading to a nearly symmetric resonant profile. Similarly, a nearly symmetric $2p^2\,{}^1S$ to $2pnd\,{}^1P$ resonant structure can be attributed directly to a strong $2p\rightarrow nd$ bound-bound excitation. In fact, our calculation has shown that the photoionization from an initial state with a large $2pnp$ mixing is always dominated by a nearly sym-

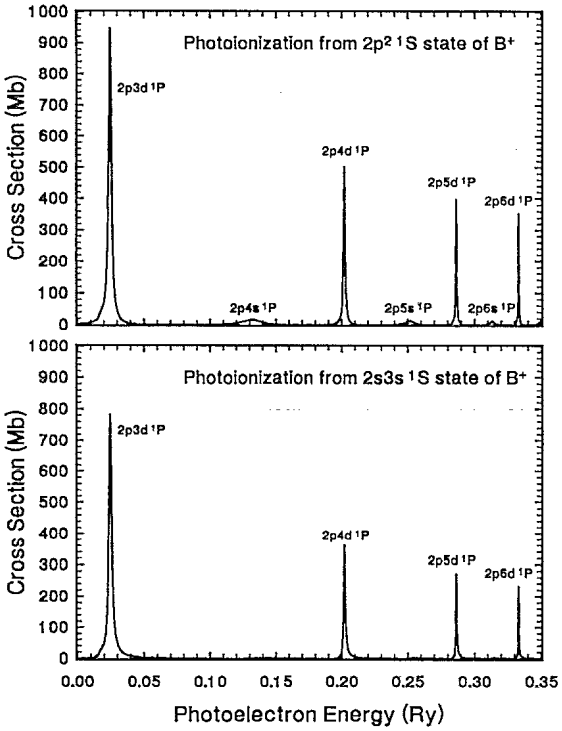

FIG. 4. Photoionization spectra from $2p^2\,{}^1S$ and $2s3s\,{}^1S$ states of Be-like B II.

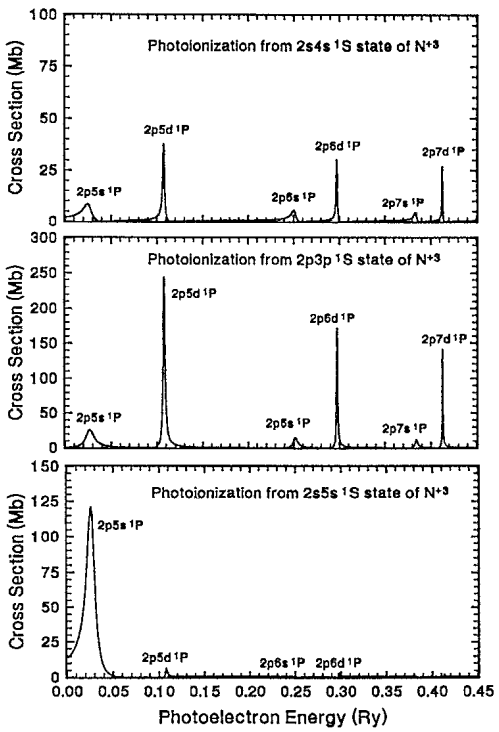

FIG. 6. Photoionization spectra from $2s4s\,{}^1S$, $2p3p\,{}^1S$, and $2s5s\,{}^1S$ states of Be-like N IV.

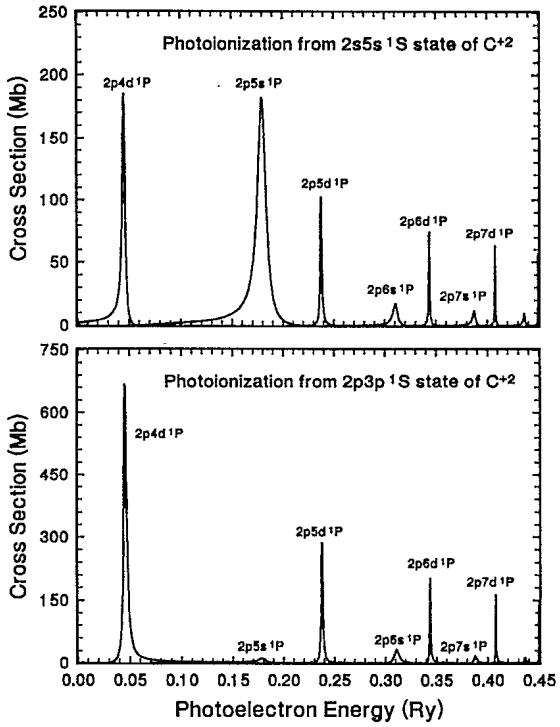

FIG. 7. Photoionization spectra from $2s5s\ ^1S$ and $2p3p\ ^1S$ states of Be-like C III.

metric $2pnd\ ^1P$ resonant series. This is also illustrated by the photoionization spectra of the B II ion shown in Fig. 4 from its $2p^2\ ^1S$ and $2s3s\ ^1S$ states with a $2p^2$ mixing of 54% and 40%, respectively.

For higher $2sns\ ^1S$ bound excited states with a small $2pp$ mixing, the photoionization spectra is dominated by the $2s \rightarrow 2p$ one-electron inner shell excitation followed by the shake-up of the outer ns electron. This is similar to the two-electron excitation of the core electron studied elsewhere [21]. Figure 5 represents the photoionization dominated by the $2sn\,(4-6)s\ ^1S$ to $2pn\,(4-6)s\ ^1P$ shake-up process of the B II ion. Unlike the $2s3s\ ^1S$ spectrum shown in Fig. 4, the $2pnd\ ^1P$ structures are barely visible in the $2sn\,(4-6)s\ ^1S$ spectra due to the small $2pnp$ mixing, i.e., approximately 2.5%, 1.3%, and 1.0% in the $2s4s\ ^1S$, $2s5s\ ^1S$, and $2s6s\ ^1S$ states, respectively. Theoretically, for transitions with nearly constant oscillator strengths, the peak cross sections of the resonant structures are inversely proportional to the resonant widths Γ [22]. Since Γ is approximately proportional to ν^{-3}, the peak cross section should approach a ν^3 dependence as the effective principal quantum number ν increases along the $2pns\ ^1P$ autoionization series if the oscillator strength is close to a constant. The fact that the peak cross sections of the $2pn\,(\geq 4)s\ ^1P$ resonances shown in Fig. 5 increase approximately as ν^3 supports quantitatively that the $2sn\,(\geq 4)s\ ^1S$ to $2pn\,(\geq 4)s\ ^1P$ photoionization is indeed dominated by the one-electron $2s \rightarrow 2p$ excitation followed by the shake-up of the outer ns electron.

For a transition from an initial state with a medium $2pp$ mixing, the peak cross section of a $2pnd\ ^1P$ resonance is usually fairly modest (e.g., ~50 Mb or less) in comparison to the larger peak photoionization cross section (e.g., 100 Mb or, often, substantially larger) from an initial state with a larger $2pp$ mixing. This is illustrated by the $2pnd\ ^1P$ resonances in the N IV $2s4s\ ^1S$ photoionization spectrum shown in Fig. 6. (The N IV $2s4s\ ^1S$ state is approximately an 83.4% $2s4s$ and 16.5% $2p3p$ mixture.). In contrast, the peak cross sections for the $2pnd\ ^1P$ resonances in the $2p3p\ ^1S$ spectrum are significantly larger due to a 22% $2s4s$ and 77.8% $2p3p$ mixture in the $2p3p\ ^1S$ state. The N IV $2s5s\ ^1S$ photoionization spectrum

TABLE II. The effective principal quantum number ν and the resonant widths Γ (in $a[-b]=a\times10^{-b}$ Ry) of selected doubly excited $2pvs\ ^1P$ autoionization series of the Be isoelectronic sequence below the $2p\ ^2P$ threshold. The listed ν is derived against the $2p\ ^2P$ threshold listed in Table I.

State	Γ	ν	State	Γ	ν	State	Γ	ν
	Be			B^+			C^{2+}	
$2p3s$	3.81[−2]	2.4076	$2p4s$	1.82[−2]	3.6014	$2p5s$	9.57[−3]	4.6943
$2p4s$	1.24[−2]	3.4106	$2p5s$	8.11[−3]	4.6003	$2p6s$	5.09[−3]	5.6930
$2p5s$	5.54[−3]	4.4100	$2p6s$	4.35[−3]	5.5995	$2p7s$	3.07[−3]	6.6930
$2p6s$	2.98[−3]	5.4043	$2p7s$	2.60[−3]	6.5994	$2p8s$	1.99[−3]	7.6925
			$2p8s$	1.68[−3]	7.5994	$2p9s$	1.36[−3]	8.6925
	N^{3+}			O^{4+}			F^{5+}	
$2p5s$	1.08[−2]	4.7515	$2p6s$	6.24[−3]	5.7900	$2p7s$	4.01[−3]	6.8180
$2p6s$	5.82[−3]	5.7509	$2p7s$	3.78[−3]	6.7896	$2p8s$	2.58[−3]	7.8180
$2p7s$	3.46[−3]	6.7506	$2p8s$	2.42[−3]	7.7896	$2p9s$	1.77[−3]	8.8177
$2p8s$	2.23[−3]	7.7503	$2p9s$	1.65[−3]	8.7894	$2p10s$	1.26[−3]	9.8177
$2p9s$	1.53[−3]	8.7501	$2p10s$	1.18[−3]	9.7894	$2p11s$	9.33[−4]	10.8177
	Ne^{6+}			Na^{7+}			Mg^{8+}	
$2p7s$	4.21[−3]	6.8396	$2p8s$	2.85[−3]	7.8562	$2p8s$	2.94[−3]	7.8696
$2p8s$	2.73[−3]	7.8395	$2p9s$	1.95[−3]	8.8561	$2p9s$	2.02[−3]	8.8696
$2p9s$	1.86[−3]	8.8393	$2p10s$	1.40[−3]	9.8561	$2p10s$	1.45[−3]	9.8695
$2p10s$	1.34[−3]	9.8394	$2p11s$	1.04[−3]	10.8561	$2p11s$	1.07[−3]	10.8695
$2p11s$	9.89[−4]	10.8393	$2p12s$	7.88[−4]	11.8560	$2p12s$	8.18[−4]	11.8695

TABLE III. The effective principal quantum number ν and the resonant widths Γ (in $a[-b]=a\times10^{-b}$ Ry) of selected doubly excited $2p\nu d\ ^1P$ autoionization series of the Be isoelectronic sequence below the $2p\ ^2P$ threshold. The listed ν is derived against the $2p\ ^2P$ threshold listed in Table I.

State	Γ	ν	State	Γ	ν	State	Γ	ν
	Be			B^+			C^{2+}	
$2p3d$	2.80[−5]	3.0978	$2p3d$	2.53[−3]	3.0948	$2p4d$	3.07[−3]	4.0687
$2p4d$	2.05[−5]	4.0962	$2p4d$	1.28[−3]	4.0883	$2p5d$	1.63[−3]	5.0640
$2p5d$	1.41[−5]	5.0952	$2p5d$	7.14[−4]	5.0849	$2p6d$	9.52[−4]	6.0615
			$2p6d$	4.37[−4]	6.0832	$2p7d$	6.05[−4]	7.0599
			$2p7d$	2.82[−4]	7.0824	$2p8d$	4.06[−4]	8.0588
	N^{3+}			O^{4+}			F^{5+}	
$2p5d$	2.31[−3]	5.0495	$2p6d$	1.62[−3]	6.0372	$2p6d$	1.80[−3]	6.0305
$2p6d$	1.35[−3]	6.0469	$2p7d$	1.02[−3]	7.0357	$2p7d$	1.12[−3]	7.0291
$2p7d$	8.49[−4]	7.0454	$2p8d$	6.73[−4]	8.0349	$2p8d$	7.34[−4]	8.0285
$2p8d$	5.69[−4]	8.0443	$2p9d$	4.76[−4]	9.0342	$2p9d$	5.12[−4]	9.0278
$2p9d$	4.00[−4]	9.0436	$2p10d$	3.43[−4]	10.0334	$2p10d$	3.73[−4]	10.0276
	Ne^{6+}			Na^{7+}			Mg^{8+}	
$2p7d$	1.22[−3]	7.0248	$2p7d$	1.26[−3]	7.0215	$2p8d$	8.89[−4]	8.0180
$2p8d$	8.03[−4]	8.0241	$2p8d$	8.39[−4]	8.0207	$2p9d$	6.17[−4]	9.0176
$2p9d$	5.61[−4]	9.0235	$2p9d$	5.88[−4]	9.0202	$2p10d$	4.46[−4]	10.0173
2p10d	4.06[−4]	10.0231	$2p10d$	4.23[−4]	10.0199	$2p11d$	3.33[−4]	11.0171
$2p11d$	3.03[−4]	11.0229	$2p11d$	3.18[−4]	11.0197	$2p12d$	2.55[−4]	12.0169

represents a typical shake-up process of the $5s$ electron following the $2s\rightarrow2p$ excitation as the $2pnp$ mixing in the initial state is reduced to 3.8%.

Figure 7 presents a very strong $2s5s\ ^1S$ to $2p5s\ ^1P$ photoionization of Be-like C III. This transition is dominated by the combined contribution of a bound-bound $2pnp\rightarrow2p5s$ transition (or a $np\rightarrow5s$ one-electron excitation) and the shake-up of the $5s$ electron following the one-electron $2s\rightarrow2p$ excitation. The cross section to the $2p5s\ ^1P$ resonance is substantially reduced in the $2p3p\ ^1S$ photoionization spectrum, while other $2pns\ ^1P$ resonances remain strong due to a shift of the $2sns$ mixing in the $2p3p\ ^1S$ state from $2s5s$ to $2sn(\geq6)s$ configurations. Similar to some of the spectra shown earlier, the large $2pnp$ mixing (i.e., approximately 24.7% according to our calculation) in the $2s5s\ ^1S$ state is responsible for the presence of the dominating $2pnd\ ^1P$ and the clearly visible $2pn(\geq6)s\ ^1P$ autoionization series. We also note that the ratios of the $2pn(\geq5)d\ ^1P$ peak photoionization cross sections between $2p3p\ ^1S$ and $2s5s\ ^1S$ spectra is approximately 2.7, which is very close to the ratio of 2.6 between the $2p3p$ components in the $2p3p\ ^1S$ and $2s5s\ ^1S$ initial state, i.e., 63.9% and 24.7%, respectively.

B. Resonant widths

In Tables II and III, we present the resonant widths of a few selected doubly excited $2pns\ ^1P$ and $2pnd\ ^1P$ autoionization states of Be isoelectronic sequence below the $2p\ ^2P$ threshold. The effective principal quantum numbers ν, which are derived against the $2p\ ^2P$ threshold given in Table I, of both $2pns\ ^1P$ and $2pnd\ ^1P$ series for Be-like ions up to Mg^{+8} are also listed. Except for Be I, the widths of the $2pns\ ^1P$ series are in general a few times to a factor of 10 greater than the widths of the $2pnd\ ^1P$ series. For Be I, the widths of the $2pns\ ^1P$ series are over two orders of magnitude greater than the widths of the $2pnd\ ^1P$ series. Figure 8 presents the calculated resonant widths, expressed in terms of the product of Γ and ν^3 as functions of effective principal quantum number ν, of the $2pns\ ^1P$ and $2pnd\ ^1P$ series for the Be isoelectronic se-

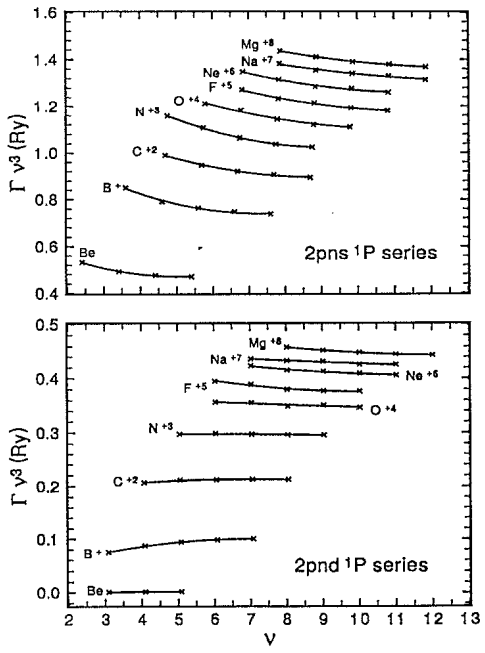

FIG. 8. The variation of the product of resonant width Γ and ν^3 as a function of the effective principal quantum number ν for the $2pns\ ^1P$ and $2pnd\ ^1P$ autoionization series of Be-like ions. The solid curve represents a least-squares fit of the calculated Γ to Eq. (7).

quences up to Mg^{+8}. The theoretical widths appear to follow qualitatively the expression [8]

$$\sum_{i=1} \frac{a_i}{\nu^{2i+1}} , \tag{7}$$

where a_i are constants. As expected, Γ approaches a ν^3 dependence as ν increases along the autoionization series. The slow increase in resonant width Γ for a specific $2pnl\ ^1P$ resonance along the isoelectronic sequence, except for the $2pnd\ ^1P$ series of Be I, suggests a slow increase of the interaction strength between the $2pnl$ bound component and the $2s\epsilon p$ continuum component of the final-state wave function as the effective nuclear charge Z_{eff} increases. The small quantum defect for the $2pnd\ ^1P$ series indicates that the relative narrow $2pnd\ ^1P$ series is essentially quasihydrogenic.

IV. CONCLUSIONS

The theoretical photoionization spectra of Be isoelectronic sequence presented in this study allow us to examine in detail the variation of the resonant structure of doubly excited resonance, both individually and collectively in an autoionization series. The relative contribution (or the interference) between the bound-bound and bound-continuum transitions is measured by the asymmetry parameter q, which manifests itself in terms of the degree of symmetry of the resonant profile. Except for the photoionization from the ground state, most of the strong transitions can be linked directly to the one-electron bound-bound excitations with a nearly symmetric structure profile shown in Figs. 3–7. In addition, our calculation has shown that the initial-state configuration mixing is responsible for the presence of strong resonances such as the $2pnd\ ^1P$ series shown in Figs. 4, 6, and 7.

ACKNOWLEDGMENT

This work was supported by NSF under Grant Nos. PHY91-11420 and PHY94-13338.

[1] S. Chu, J. E. Bjorkholm, A. Ashkin, and A. Cable, Phys. Rev. Lett. **57**, 314 (1986).
[2] J. P. Briand, P. Charles, J. Arianer, H. Laurent, C. Goldstein, J. Dubau, M. Loulergue, and F. Bely-Dubau, Phys. Rev. Lett. **52**, 617 (1984).
[3] R. E. Marrs, M. A. Levine, D. A. Knapp, and J. R. Henderson, Phys. Rev. Lett. **60**, 1715 (1988).
[4] F. J. Wuilleumier, in *Many-Body Theory of Atomic Structure and Photoionization,* edited by T. N. Chang (World Scientific, Singapore, 1993), p. 349.
[5] T. N. Chang and R. Q. Wang, Phys. Rev. A **44**, 80 (1991).
[6] U. Fano, Phys. Rev. **124**, 1866 (1961).
[7] M. J. Seaton, Proc. Phys. Soc. London **88**, 801 (1966).
[8] T. N. Chang, J. Phys. B **11**, L583 (1978).
[9] T. N. Chang and X. Tang, Phys. Rev. A **44**, 232 (1991).
[10] T. N. Chang, in *Many-Body Theory of Atomic Structure and Photoionization* (Ref. [4]), p. 213.
[11] T. N. Chang and Y. S. Kim, Phys. Rev. A **34**, 2609 (1986).
[12] T. N. Chang, Phys. Rev. A **39**, 4946 (1988).
[13] T. N. Chang and K. T. Chung, Chin. J. Phys. **27**, 425 (1989).
[14] A. Burgess, Proc. Phys. Soc. **81**, 442 (1963).
[15] P. G. Burke and D. D. McVicar, Proc. R. Soc. London **86**, 989 (1965).
[16] G. N. Bates and P. L. Altick, J. Phys. B **6**, 653 (1973); T. N. Chang, Phys. Rev. A **34**, 4554 (1986).
[17] T. N. Chang, Phys. Rev. A **36**, 447 (1987).
[18] T. N. Chang and L. Zhu, Phys. Rev. A **48**, R1725 (1993).
[19] C. E. Moore, *Atomic Energy Levels,* Natl. Bur. Stand. (U.S.) Circ. No. 467 (U.S. GPO, Washington, D.C., 1949), Vol. I; L. Johansson, Phys. Scr. **19**, 236 (1974); C. E. Moore, *Selected Tables of Atomic Spectra. Atomic Energy Levels and Multiplet Tables, C_I–C_{VI},* NSRDS-NBS 3, Sec. 3 (U.S. GPO Washington, D.C., 1971), p. A6 IV-1; *Selected Tables of Atomic Spectra,* NSRDS-NBS 3, Sec. 4 (U.S., GPO, Washington, D.C., 1971); W. C. Martin and R. Zalubas, J. Phys. Chem. Ref. Data **9**, 1 (1980).
[20] T. N. Chang and Y. Mu, J. Quant. Spectrosc. Radiat. Transfer **44**, 413 (1990).
[21] R. M. Jopson, R. R. Freeman, W. E. Cooke, and J. Bokor, Phys. Rev. Lett. **51**, 1640 (1983).
[22] T. N. Chang, Phys. Rev. A **37**, 4090 (1988).